Investigation of vortex packet recovery in perturbed turbulent boundary layers

Yan Ming Tan[1], Ellen K. Longmire[2]

Department of Aerospace Engineering and Mechanics
University of Minnesota, Minneapolis, MN, 55455 USA
[1]tanxx247@umn.edu
[2]longmire@umn.edu

ABSTRACT

Turbulent boundary layers (Re_τ = 2500) were perturbed by a spanwise array of cylinders with spacing of S= 0.2δ, where δ is the unperturbed boundary layer thickness. Two cylinder heights were considered, H = 0.2δ (H^+ = 500) and H = δ. Although visualizations suggest that disrupted packet signatures downstream of the H = δ array re-organized from bottom up, autocorrelation magnitudes along the streamwise direction for the flow at z^+ = 125 were reduced relative to unperturbed values up to 7δ downstream of the array suggesting that flow features unrelated to packets remained altered there. On the other hand, spectral energy in large spanwise scales recovered substantially at the same location. For the H = 0.2δ case, previous results showed disrupted packet signatures re-appearing beginning 2δ downstream at z^+ = 300, while packet signatures at z^+ = 500 persisted through the array, supporting a top-down reorganization. However, spanwise characteristics of flow features closer to the wall (z^+ = 125) remained altered relative to the unperturbed flow up to 7δ downstream yet streamwise length scales from autocorrelations at z^+ = 125 and x = 7δ matched unperturbed values. Interestingly, the shape of the spanwise energy spectrum at this location resembled shapes of spectra in planes above, suggesting outer-layer influence.

INTRODUCTION

Vortex packets, which are characterized by multiple hairpins aligned in the streamwise direction moving downstream at a relatively uniform convection velocity (Adrian *et al.* 2000; Tomkins & Adrian 2003), have been shown to contribute significantly to the Reynolds stresses within the logarithmic layer despite occupying a relatively small area (Ganapathisubramani *et al.* 2003). Velocity statistics within turbulent boundary layers have been represented accurately by a hierarchy of eddies in the form of vortex packets using Townsend's attached eddy hypothesis (e.g. Perry & Chong 1982; de Silva *et al.*2016). Furthermore, the large-scale organization in the logarithmic layer, predominantly in the form of packets, seems to significantly influence the small-scale fluctuations closer to the wall (Hutchins & Marusic, 2007). Therefore, perturbing the packet organization within the logarithmic layer may be a viable means of manipulating boundary layer behavior.

Various studies have sought to perturb turbulent boundary layers, often for the purpose of reducing skin friction drag. These studies can be grouped broadly into two categories: 1) manipulating near-wall structures via surface roughness/non-uniformities (e.g. Flack & Schultz 2014, Nugroho *et al.* 2013) and 2) altering the large-scale energy containing motions within and outside of the logarithmic region. The present study falls into the latter group, and follows a number of previous studies. For example, Corke *et al*. (1981) investigated large eddy breakup devices in the form of wall-parallel flat plates that extended to H/δ = 0.8 in a $Re_\tau \sim 1900$ TBL and reported skin friction drag reductions of up to 30-40%. Separately, Tomkins (2001) showed that arrays of hemispheres (H/δ = 0.09) reduced streamwise length scales of flow structures above the array height.

The present study follows on previous work by Ryan *et al.* (2011), Ortiz-Dueñas *et al.* (2011) and Zheng & Longmire (2014) perturbing the logarithmic layer in a boundary layer with Re_τ = 2500 using a spanwise array of cylinders (H/δ = 0.2, H^+ = 500). The previous results showed profound effects on velocity statistics and flow organization downstream of the perturbations. PIV measurements at a wall-normal location of z^+ = 300 by Zheng & Longmire (2014) showed that a cylinder array with spacing S = 0.2δ first disrupted incoming packet signatures downstream. However, the upstream packet signatures reappeared within 2δ downstream at similar spanwise locations. They hypothesized that the reappearance was due to the influence of the unperturbed packet organization above the array.

To investigate the aforementioned hypothesis, Tan & Longmire (2017) devised and applied a vortex packet identification algorithm (VPIA) to planar PIV measurements at three discrete measurement heights, z^+= 125, 300 and 500 downstream of similar perturbations, and an additional S = 0.2δ array consisting of cylinders with height, H = δ. The aim was to quantify recovery of packet signatures downstream of both the arrays investigated. Relaxation trends differed substantially between the two arrays. Downstream of the H = δ array, both instantaneous PIV and VPIA results showed a bottom up mechanism for the recovery of large-scale flow organization. On the other hand, although results did indicate some signs of top-down recovery downstream of the H = 0.2δ array, the overall picture was not so clear as at z^+ = 125 flow structures differed relative to those in unperturbed flow until 7δ downstream.

The present paper investigates the aforementioned trends further by considering energy spectra and autocorrelations downstream of both arrays.

EXPERIMENT SETUP

All measurements were acquired in a water channel facility. A trip wire 6m upstream of the first measurement location initiated the turbulent boundary layer, which developed along the bottom wall of the channel. At x = 0, corresponding to the cylinder array location in perturbed cases, the unperturbed boundary layer thickness, δ was 125.5 mm and Re_τ was 2500. The free-stream

velocity, U_∞ was 0.508 m/s. More details on the measurement facility can be found in Gao (2011).

Two cylinder arrays spaced at S = 0.2δ with cylinder heights of H = 0.2δ (H^+ = 500, aspect ratio, AR = 4) and δ (H^+ = 2500, AR = 20) were investigated. The cylinder diameters were D = 6.35mm.

Planar PIV measurements were acquired in three wall-parallel planes, z^+ = 125, 300 and 500 and six streamwise locations covering a distance of 0 < x < 7.5δ. Two TSI 4MP Powerview cameras were used simultaneously to acquire a field of view that was 1.1δ × 2.1δ in the streamwise and spanwise directions respectively. The PIV resolution was 2.2 mm (l^+ = 40) while the vector spacing at 50% overlap was 1.1 mm (l^+ = 20). A total of 1000 independent samples were acquired for each measurement location at a rate of 0.5 Hz. The uncertainties for the instantaneous vectors in both streamwise and spanwise directions were estimated to be $0.01U_\infty$.

Separately, a 3-D PTV system was used to measure volumetric velocity fields in unperturbed flow and flow perturbed by the cylinders. For the H = 0.2δ case, measurement volumes covered 0.1 < x/δ < 0.8, 2 < x/δ < 2.7 and 3.3 < x/δ < 4. For H = δ, the locations spanned 0.1 < x/δ < 0.8, 2.2 < x/δ < 2.9 and 4.3 < x/δ < 5.0.

Four TSI 8MP PowerView cameras fitted with Scheimpflug mounts were used to acquire measurement volumes encompassing 155 < z^+ < 465 within the logarithmic layer. Particle tracks were acquired using a robust point matching technique described in Stellmacher & Obermayer (2000) to arrive at a volumetric velocity field, which contained roughly 35,000 to 55,000 randomly spaced vectors. The volumes were then interpolated using Gaussian-weighting with a 0.7 ratio between the Gaussian radius and the node volume half-size, onto a rectangular grid with node dimensions of 7 mm × 4 mm × 3 mm (138 × 78 × 60 wall units) in the streamwise, spanwise, and wall normal directions, respectively, with a node volume overlap of 75%. 500 independent volumes were acquired at a rate of 0.5 Hz. The estimated uncertainties for the particle tracks were $0.01U_\infty$ for both streamwise and spanwise velocity components while being larger for the wall-normal velocity component at $0.03U_\infty$.

Results

Unperturbed flow

Figure 1 shows instantaneous PIV fields from unperturbed flow acquired at the three measurement heights. Hairpin packet signatures appear as streamwise coherent slow moving regions (blue) bounded by counter-rotating swirling structures (depicted by black and green contours), following the definition of Tomkins & Adrian (2003). Packet signatures observed at z^+ = 125 (Fig. 1a) were typically long and narrow. At z^+ = 300 (Fig. 1b), packet signatures became wider with fewer swirling structures. These trends continued at z^+ = 500 (Fig. 1c). Generally, packet signatures became wider with increasing measurement height, consistent with the results of Tomkins & Adrian (2003).

Perturbed flow, S = 0.2δ, H = 0.2δ array

The flow immediately downstream of the H = 0.2δ cylinders was highly three-dimensional. Figure 2 shows the time-averaged streamwise velocity immediately downstream of the H = 0.2δ cylinders. On average, wakes appear immediately behind each cylinder, with fast moving zones in the regions between. The regions marked by iso-surfaces slower than 0.95$\bar{U}$ tapered off

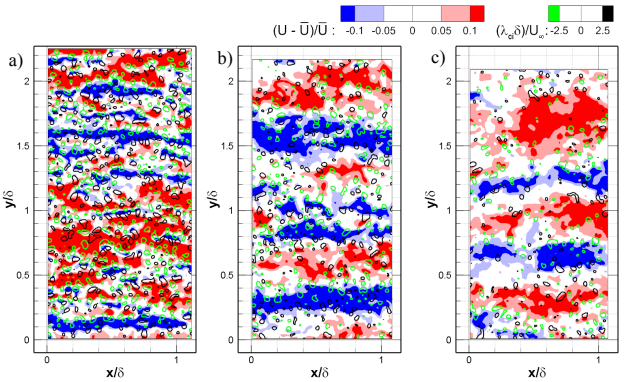

Fig. 1. Unperturbed flow. Instantaneous vector fields from PPIV at a) z^+ = 125, b) z^+= 300 and c) z^+ = 500. Blue and red contours show deviation from local mean velocity at the measurement height, and normalized by the same local mean velocity.

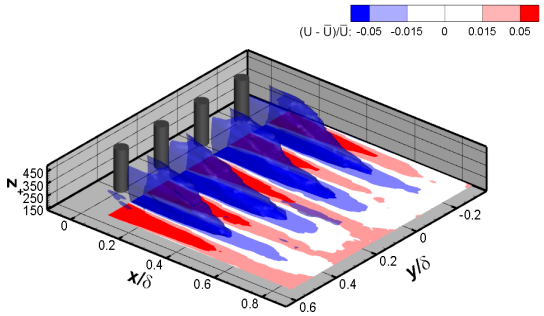

Fig. 2. S = 0.2δ, H = 0.2δ array. Average streamwise velocity results from 3-D PTV. Colors at z^+ = 155 show fractional deviation away from the local mean velocity. Iso-surfaces show regions with U < 0.95$\bar{U}$.

with increasing z as the streamwise velocity deficit decreased. This was due to the downwash effect initiated at the tips of the cylinders, drawing faster moving fluid towards the wall (see Fig. 3b). The downwash effect also extends to z^+ = 300 (Fig. 3a) on average. At z^+ = 500, the downwash effect resulted in fast moving zones on average that were aligned with cylinder locations (Fig. 4c). Furthermore, at z^+ = 300, the initial average velocity deficit close to the cylinders split with fast moving zones forming behind the cylinders beginning at x = 0.3δ, while the slow moving zones shift to the regions between cylinders (Fig. 4b). In contrast, the wake splitting effect was less evident closer to the wall at z^+ = 125 (Fig. 4a), suggesting that downwash effects had not extended there yet.

The H = 0.2δ array perturbed the incoming flow the least at z^+= 500, such that incoming packet signatures tended to persist downstream (Tan & Longmire 2015). In contrast, at z^+ = 300, packet signatures were initially disrupted in the region immediately downstream of the array, but reappeared rapidly by x = 2δ in roughly similar spanwise locations (see also Zheng & Longmire 2014). The aforementioned trends at z^+ = 300 and 500 support a top down recovery mechanism. The behavior at z^+ = 125 suggested otherwise, where surprisingly, packet signatures remained altered beyond the last measurement station at x = 7δ. Figure 5 shows the evolution of the flow features at z^+ = 125 with

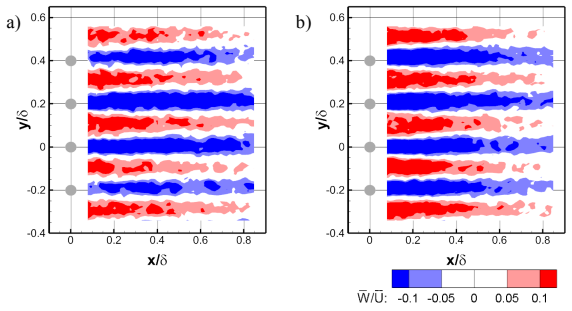

Fig. 3. S = 0.2δ, H = 0.2δ array. Streamwise-spanwise slices of average wall-normal velocity from 3-D PTV at a) z^+ = 300 and b) z^+ = 465.

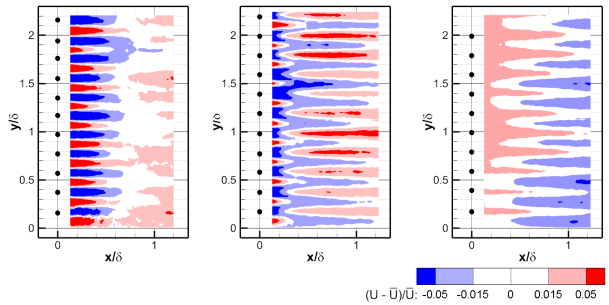

Fig. 4. S = 0.2δ, H = 0.2δ array. Average streamwise velocity results from PIV at measurement height a) z^+ = 125, b) z^+ = 300 and c) z^+ = 500.

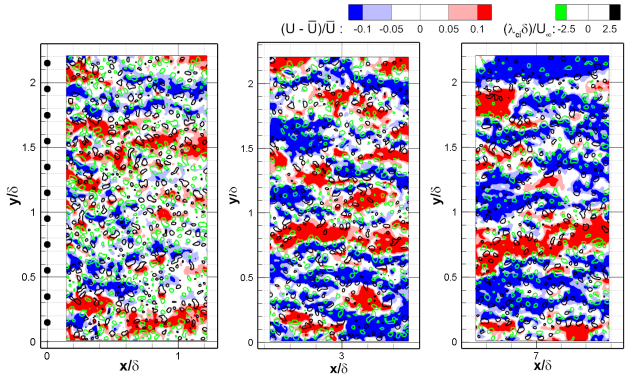

Fig. 5. S = 0.2δ, H = 0.2δ. Instantaneous fields from PIV at z^+ = 125, centered at a) x = 0.7δ, b) x = 2.9δ and c) x = 7δ.

increasing distance downstream of the H = 0.2δ array. Immediately downstream of the array, Karman-like wake structures were dominant, obscuring any packet signatures (Fig. 5a). Wakes were observed at y/δ = 0.15, 0.55, and 1.95.

Also, neighboring wakes often interact, for example at y/δ = 0.95 and 1.15. As x increased, long low momentum regions (LMRs) appeared wavy and unlike packet signatures in the unperturbed flow. For example at x = 2.9δ (Fig. 5b), wavy structures were connected to spanwise adjacent ones, as in y/δ = 0.3. Some of these wavy low momentum structures persisted until x = 7δ, and likely beyond, although the undulation amplitude tended to decrease. Still, many spanwise merged or merging structures remained, as seen at y/δ = 0.4, 1.1 and 1.6 in Fig. 5c. Thus, the H = 0.2δ array profoundly affected the spanwise organization of packet signatures at z^+ = 125, with effects lasting until x = 7δ.

Perturbed flow, S = 0.2δ, H = δ array

The averaged and instantaneous streamwise velocity trends downstream of the H = δ array was quite different compared to the H = 0.2δ array. For all the measurement heights, strong wakes occurred behind each cylinder. Furthermore, no average wake splitting was observed. When streamwise velocity was averaged across the span, the larger blockage of the taller cylinders resulted in sustained overall velocity deficits throughout the logarithmic layer beyond x = 7δ, in contrast with the H = 0.2δ case, where streamwise velocity statistics relaxed towards the unperturbed values over this distance (Tan 2017).

At z^+ = 125 and 300, the individual wake signatures were qualitatively similar to those observed downstream of the H = 0.2δ array, even though mean velocity statistics differed (see Tan & Longmire 2017). LMRs associated with wakes often appeared short and wavy at all measurement heights (see Figs. 6a,7a & 8a). Often, individual wakes would interact with adjacent ones, for example at z^+ = 125, y/δ = 1.35 and 1.55, z^+ = 300, y/δ = 1.1 and 1.3, and z^+ = 500, y/δ = 1.35 and 1.55. Remarkably, at z^+ = 125 and x/δ = 2.9 (Fig. 6b), the flow structures downstream of the H = δ array were relatively similar to those in unperturbed flow, and unlike the structures observed at the same location downstream of the H = 0.2δ array (compare Figs. 6b & 5b to unperturbed flow in Fig. 1a). For the H = δ case, packets similar to those in the unperturbed flow were observed beginning at this streamwise location, as in Figure 6b at y/δ = 0.15, 0.3, 1.0 and 2.0. At this height, the packet signatures became more similar to those in unperturbed flow with increasing x, such that they became less wavy and frequently longer than packet signatures upstream, for example in Fig. 6c at y/δ = 0.3, 0.5, 1.0 and 1.3.

At z^+ = 300 and 500, in contrast, packet signatures were hardly ever observed at x = 2.9δ downstream of the H = δ array. The LMRs there often appeared disorganized, wavy, short and lacked obvious paired counter-rotating swirls. Examples at z^+ = 300 (Fig. 7b, y/δ = 0.7, 1.2 and 1.8) and at z^+ = 500 (Fig. 8b, y/δ = 0.7 and 1.5) reflect this behavior. At x/ δ = 7 and z^+ = 300, some packets similar to those in unperturbed flow were observable (e.g. at y/δ = 1.1 in Fig. 7c). In comparison, at z^+ = 500 (Fig. 8c), packets similar to those in the unperturbed flow were still hardly ever observed. Any packet-like structures tended to look narrower and shorter than those in the unperturbed flow (see Figure 7c at y/δ = 1.9 and possibly 2.0). The flow organization here was substantially different from the flow downstream of the H = 0.2δ array.

STATISTICAL ANALYSES

Autocorrelations of streamwise velocity along the streamwise direction (Δy = 0) are shown in Figure 9 for both arrays and all measurement heights. Immediately downstream of the H = 0.2δ array (Fig. 9a-c), autocorrelation magnitudes were reduced. The largest reduction was at z^+ = 125 (Fig. 9a) and the least at z^+ = 500 (Fig. 9c). This result suggests that the array disrupted existing flow structures by shortening them, with the effect diminishing as the tip of the cylinder was approached.

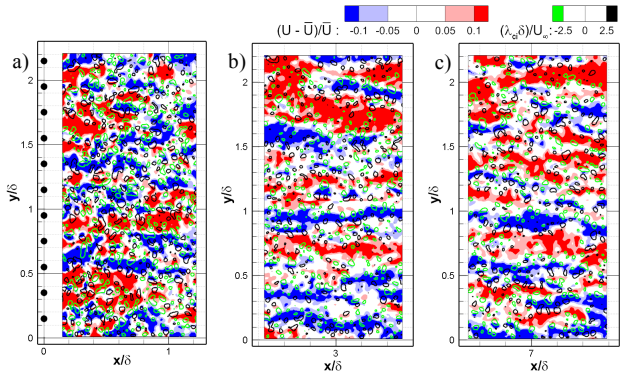

Figure 6. S = 0.2δ, H = δ. Instantaneous fields from PIV at z^+ = 125, centered at a) x = 0.7δ, b) x = 2.9δ and c) x = 7δ.

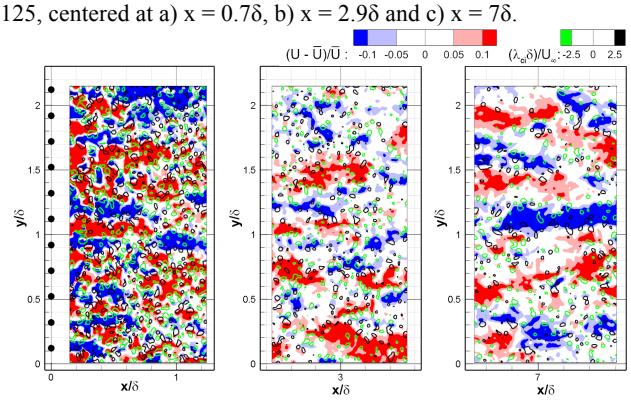

Fig. 7. S = 0.2δ, H = δ array. Instantaneous fields from PIV at z^+ = 300 centered at a) x = 0.7δ, b) x = 2.9δ and c) x = 7δ.

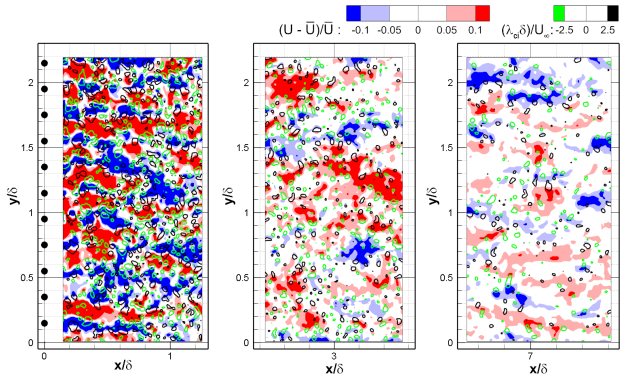

Fig. 8. S = 0.2δ, H = δ. Instantaneous fields from PIV at z^+ = 500, centered at a) x = 0.7δ, b) x = 2.9δ and c) x = 7δ.

As x increased, both the shapes and magnitudes of the autocorrelations recovered substantially towards unperturbed values. In general, recovery occured earlier for smaller Δx, then later for larger Δx at all measurement heights. Physically, this is reasonable since longer structures are associated with larger time scales (Smits & Wood 1985), hence it would take a longer time for the longer structures to re-organize. At x = 1.8δ, z^+ = 125(not shown), the correlation magnitudes for |Δx| < 0.1δ had already recovered to the unperturbed values, in contrast to z^+ = 300 and 500, which is consistent with the shorter response times closer to the wall (Smits & Wood 1985).

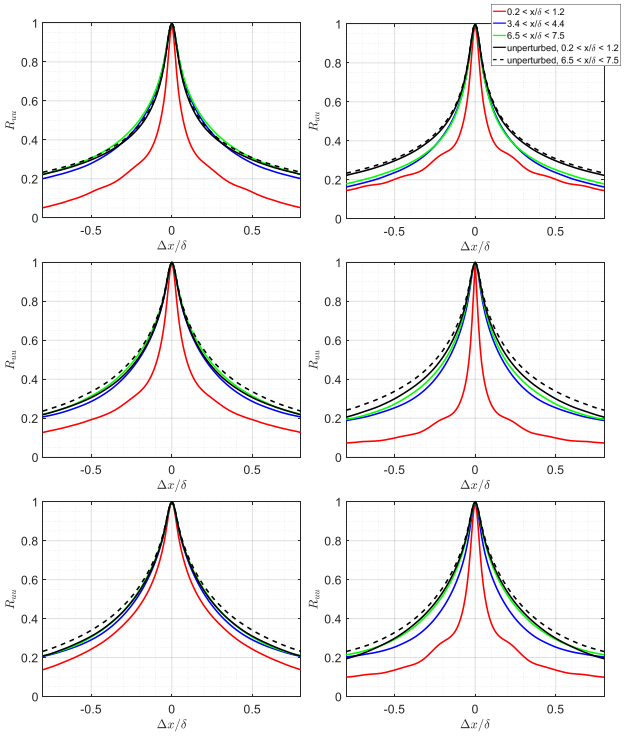

Fig. 9. Autocorrelations of streamwise velocity for Δy = 0 downstream of S = 0.2δ, H = 0.2δ array at measurement height a) z^+ = 125, b) z^+ = 300, and c) z^+ = 500. Similar plots downstream of S = 0.2δ, H = δ array aforementioned measurement heights shown in d,e,f.

Further downstream, at x = 3.9δ and z^+ = 125, correlation values exceeded unperturbed values slightly, suggesting possibly more flow content with length scales less than 0.3δ on average, which did not occur at z^+ = 300 or 500.

Finally, at x = 7δ, correlations recovered to unperturbed values at z^+ = 125 (Fig. 9c), with slight enhancement for 0.1δ < |Δx| < 0.3δ, although this effect was likely within the uncertainty. In contrast, at z^+ = 300 and 500, correlation values remained suppressed for |Δx| > 0.2δ, suggesting fewer long structures.

Trends in autocorrelations downstream of the H = δ array showed substantial differences relative to the H = 0.2δ case. Correlation magnitudes were also reduced relative to the unperturbed flow at all measurement heights, similar to the H = 0.2δ case. Different from the H = 0.2δ case, the autocorrelations magnitudes were more strongly reduced at z^+ = 500 (Fig. 9f). Furthermore, at all measurement heights, a bulge occurred close to Δx = 0.23δ. The bulge may correspond to characteristic length scales of the Karman vortices present at all measurement heights downstream of this array.

The Reynolds number based on cylinder diameter and local mean velocity varied from 2100 to 2600 across the logarithmic layer. A Strouhal number of 0.2 yields characteristic vortex shedding frequencies of 10.4 Hz and 13 Hz at z^+ = 125 and 500 respectively. Assuming that the wake vortices convect at the reduced local mean velocities immediately downstream of the array, length scales of 0.25δ and 0.23δ estimated for z^+ = 125 and 500 respectively correspond roughly to the bulge location. This

phenomenon was not evident in the H = 0.2δ case, which may indicate that tip effects disrupted or weakened the vortex shedding signatures below.

As x increased, correlations at all heights relaxed toward the shapes and values seen in the unperturbed flow. However, at x = 7δ, correlation magnitudes remained suppressed at all measurement heights, different from the H = 0.2δ case. Notably, at z^+ = 125 (Fig. 9d) and 300 (Fig. 9e), the reductions were stronger than at z^+ = 500(Fig. 9f). This was fairly surprising since the instantaneous visualizations at x = 7δ showed similar structures to those in unperturbed flow at z^+ = 125 (see Fig. 5c), while hardly any were observed at z^+ = 500 (see Fig. 7c), where regions of uniform streamwise momentum appear much shorter. This result may suggest that there were still fewer long structures relative to the unperturbed flow at z^+ = 125. Additionally, flow features not directly associated with packets (e.g. high momentum zones) may still differ substantially from those in unperturbed flow. Indeed the numbers of low and high momentum zones longer than the field of view (L > 1.05δ) were fewer at z^+ = 125 (Tan 2017) relative to the unperturbed flow, supporting the aforementioned reason for the reduced autocorrelation magnitudes.

Immediately downstream of the H= 0.2δ array, results from one-dimensional pre-multiplied spectra of spanwise variations in streamwise velocity (Figs 10a-c) showed an initial shift in energy towards smaller scales for all measurement heights. In addition, a peak at 0.2δ corresponding to the cylinder spacing was present. The peak magnitudes were comparable for both z^+ = 125 (Fig. 10a) and 300 (Fig. 10b), while smaller at z^+= 500 (Fig. 10c).

As x increased, the spectra at both z^+ = 300 and 500 (Figs. 10b & 10c) recovered quickly towards the unperturbed shapes, first for scales smaller than λ_y < 0.1δ, and later for the larger scales. At x = 7δ, both spectra had approximately recovered to the unperturbed values. In contrast, at z^+ = 125, as x increased, the energy in the small scales decreased below the unperturbed values, while the energy contained in the large scales (0.4 < λ_y/δ < 1) increased above the unperturbed values, starting at x = 1.8δ.

Remarkably, at x = 7δ, the shape of this spectrum was very similar to the shapes of the spectra at z^+ = 300 and 500, although energy contained in the smaller scales was slightly greater at z^+ = 125. This result may relate to the modulation effects of fluid motions close to the wall by large scale flow structures further out (see e.g. Hutchins & Marusic 2007).

Immediately downstream of the H = δ array, for all measurement heights, the spectral (Figs. 10d-f) energy was reduced for spanwise wavelengths greater than ~0.3δ, relative to the unperturbed spectrum. This indicates disruption of large-scale flow organization along the spanwise direction, consistent with disruption of packet signatures. The same reductions occurred immediately downstream of the H = 0.2δ array at all measurement heights, although the reduction was much stronger for the H = δ case at z^+ = 300 and 500 (compare Fig. 10e&f to 10b&c). Also, dominant peaks at λ_y = 0.2δ were observed at all measurement heights for the H = δ case with the strongest at z^+ = 500 followed by z^+ = 125 then 300. Notably, at z^+ = 125(Fig. 10d), and different from the H = 0.2δ case, the spectral energy within smaller spanwise wavelengths did not increase relative to the unperturbed flow. It did increase however at both z^+ = 300 (Fig. 10e) and 500(Fig. 10f), similar to the H = 0.2δ case.

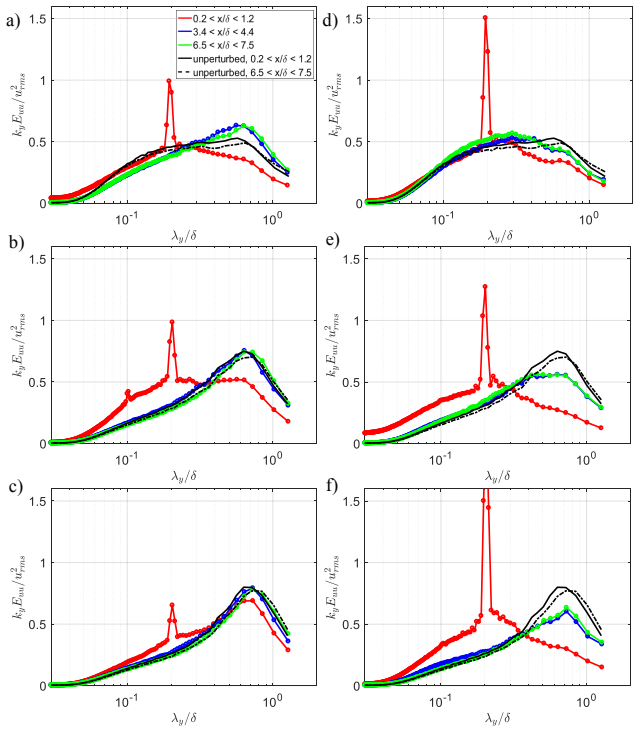

Fig. 10. 1-D pre-multiplied spectra for flow downstream of S = 0.2δ, H = 0.2δ for measurement height at a) z^+ = 125, b) z^+ = 300 and c) z^+ = 500, and flow downstream of H = δ, S = 0.2δ array with d) z^+ = 125, e) z^+ = 300 and f) z^+ = 500.

At z^+ = 300 and 500 (Figs. 10e & f), the H = δ spectra did not recover to the unperturbed shape, even at x = 7δ, different from the H = 0.2δ case. Specifically, energy contained within spanwise wavelengths greater than 0.4δ remained suppressed relative to the unperturbed values. This appears consistent with the later re-appearance of packet signatures like those in the unperturbed flow at z^+ = 300 and absence thereof at z^+ = 500, relative to z^+ = 125. In contrast, at z^+ = 125 (Figs. 10d), the spectrum shape tended towards the unperturbed shape for all spanwise wavelengths as x increased. At x = 7δ, energy levels for 0.1δ < λ_y < 0.5δ remained above the unperturbed values while spanwise wavelengths greater than 0.5δ were slightly less energetic than in unperturbed flow. Generally, at x = 7δ, the spectral values deviated the least from the unperturbed values at z^+ = 125. This trend was consistent with the re-emergence of packet signatures like those in the unperturbed flow first at z^+ = 125, which should also be accompanied by recovery of the large-scale organization across the spanwise direction, as indicated by the energy spectrum.

DISCUSSION & CONCLUSIONS

The results highlight several differences in the relaxation of the flow downstream of the two arrays. The H = δ array generated profound perturbations across the entire boundary layer thickness with prominent wavy, Karman-like wake patterns in the region immediately downstream, obscuring any packet organization throughout the log layer. In spite of the strong perturbations, packet signatures similar to those in the unperturbed flow were

observed already at $z^+ = 125$ beginning at $x \sim 2.9\delta$ and, later at $z^+ = 300$, while hardly any were seen at $z^+ = 500$. These trends suggest packet re-organization occurs from bottom up.

The pre-multiplied spectra supported this concept as, at $x = 7\delta$, the spectrum was the least perturbed at $z^+ = 125$, consistent with recovery of large-scale flow organization along the spanwise direction. However, autocorrelations along the streamwise direction at $x = 7\delta$ yielded stronger reductions at $z^+ = 125$ than at $z^+ = 500$. Flow features unrelated to packets could have contributed to this effect. Notably, visualizations indicated that both high and low uniform momentum zones (UMZs) at $z^+ = 500$ were shorter than those in unperturbed flow, while the lengths of these zones at $z^+ = 125$ appeared similar to those in the unperturbed flow. Based on these observations, we would expect autocorrelation values to be closer to unperturbed values at $z^+ = 125$ than at $z^+ = 500$. However, results from Tan (2017), who directly extracted regions of fast and slow UMZs with simple thresholds, revealed fewer long UMZs ($L > 1.05\delta$) at $z^+ = 125$ and $x = 7\delta$ than in the unperturbed flow. The relative difference was smaller than at $z^+ = 300$ and 500, supporting the trends from visualizations. Separately, the larger reductions in autocorrelation magnitudes along the streamwise direction at $z^+ = 125$ than at $z^+ = 300$ and 500 could possibly be related to changes in streamwise RMS velocity values in the perturbed flow at $x = 7\delta$ (Tan & Longmire 2017).

In the $H = 0.2\delta$ case, visualizations and spectra at $z^+ = 300$ and 500 support a top down approach to the packet organization recovery, as hypothesized by Zheng and Longmire (2014). However, the overall picture was not completely clear as flow structures close to the wall were frequently wider and connected with spanwise adjacent structures until $x = 7\delta$. Despite the difference spanwise flow variations, autocorrelations along the streamwise direction at $z^+ = 125$ and $x = 7\delta$ matched unperturbed values. This result suggests that alterations to flow structures occurred largely along the spanwise direction and that recovery trends from the autocorrelation results should be interpreted cautiously.

The persistent alterations close to the wall were likely caused by the highly three dimensional wakes of the $H = 0.2\delta$ array, where the downwash induced at the cylinder tips acts to increase wall-normal transport. At $x = 4\delta$, two-point correlations of wall-normal velocities across the depth of the log layer were increased. Wall-normal RMS velocities were also increased at all streamwise locations up to $x = 7\delta$ (Tan 2017), supporting the aforementioned claim. The increased wall-normal transport could have promoted the influence of the outer layer structures, leading to the spectrum shape at $z^+ = 125$ resembling shapes of the spectra in planes further from the wall.

In contrast to the $H = 0.2\delta$ case, the earlier recovery of flow features closer to the wall downstream of the $H = \delta$ array could be related to decreased wall-normal transport (Tan 2017). In the $H = \delta$ case, the reduced wall-normal transport was likely related to the disruption of the packet organization. Moreover, swirling zones corresponding to individual hairpins associated with ejection and sweep events that make up the vortex packet also decreased in number at all measurement heights until $x = 7\delta$, downstream of the $H = \delta$ array (Tan & Longmire 2017).

REFERENCES

Adrian, R.J., Meinhart, C.D., and Tomkins, C.D. 2000. "Vortex organization in the outer region of the turbulent boundary layer." *J. Fluid Mech.* **422**:1–54.

Corke, T.C., Guezennec Y., and Nagib, H.M. 1981. "Modification in drag of turbulent boundary layers resulting from manipulation of large-scale structures" NASA CR-3444.

de Silva, C.M, Woodcock, J.D., Hutchins, N., Marusic, I. 2016. "Influence of spatial exclusion on the statistical behavior of attached eddies", *Physical Review Fluids* 1:022401

Flack, K.A., Schultz, M.P. 2014. "Roughness effects on wall-bounded turbulent flows", *Physics of Fluids*. 26(10)

Ganapathisubramani, B., Longmire, E. K., and Marusic, I. 2003. "Characteristics of vortex packets in turbulent boundary layers." *J. Fluid Mech.***478**: 35-46.

Gao, Q. 2011. "Evolution of eddies and packets in turbulent boundary layers", Ph.D. Thesis, University of Minnesota.

Hutchins, N., Marusic, I. 2007. "Large-scale influences in near-wall turbulence", *Philosophical Transactions of the Royal Society A*. 365:647-664

Nugroho, B., Hutchins, N., and Monty, J. P. 2013. "Large-scale spanwise periodicity in a turbulent boundary layer induced by highly ordered and directional surface roughness." *International Journal of Heat and Fluid Flow* **41**:90–102.

Ortiz-Dueñas, C., Ryan, M.D., and Longmire, E. K. 2011. "Modification of Turbulent Boundary Layer Structure Using Immersed Wall-Mounted Cylinders." *Proc. Turbulent Shear Flow Phenomena VIII*, Ottawa.

Perry, A.E., Chong, M.S. 1982. "On the mechanism of wall turbulence", *J. Fluid Mech.* 119:173-217.

Ryan, M.D., Ortiz-Dueñas, C., and Longmire, E. K. 2011. "Effects of Simple Wall-Mounted Cylinder Arrangements on a Turbulent Boundary Layer." *AIAA Journal.* **49**(10):2210–2220.

Smits, A.J., Wood, D.H. 1985. "The response of turbulent boundary layers to sudden perturbations." *Annu.Rev. Fluid Mech.* 17:321-58.

Stellmacher, M., Obermayer, K. 2000. "A new particle tracking algorithm based on deterministic annealing and alternative distance measures", *Exp. Fluids*. 37:720-730.

Tan, Y.M., Longmire, E.K. 2015. "On the reorganization of perturbed hairpin packets in a turbulent boundary layer", In *9th Intl. Symp. on PIV,* Santa Barbara, California, USA.

Tan, Y.M., Troolin, D.R., Lai, W., Longmire, E.K. 2016. "Volumetric measurements of vortex packet recovery downstream of a perturbation", In *18th Intl. Symp. on Applications of Laser Imaging Techniques to Fluid Mechanics,* Lisbon, Portugal.

Tan, Y.M., Longmire, E.K. 2017. "Recovery of vortex packet organization in perturbed turbulent boundary layers", *Physical Review Fluids*. In review.

Tan, Y.M. 2017. "Turbulent boundary layers perturbed by an array of cylinders". Ph.D. Thesis, University of Minnesota.

Tomkins, C.D., 2001. "The structure of turbulence over smooth and rough walls". Ph.D. Thesis, University of Illionois, Urbana-Champaign.

Tomkins, C.D., Adrian, R.J. 2003. "Spanwise structure and scale growth in turbulent boundary layers." *J. Fluid Mech.* **490**: 37-74.

Zheng, S., and Longmire. E. K. 2014. "Perturbing vortex packets in a turbulent boundary layer." *J. Fluid Mech.* **748**:368–398.